ACS APPLIED MATERIALS & INTERFACES

Research Article

Cite This: ACS Appl. Mater. Interfaces 2019, 11, 12854−12862

www.acsami.org

Membranes with Functionalized Nanopores for Aromaticity-Based Separation of Small Molecules

Ilin Sadeghi and Ayse Asatekin*

Chemical and Biological Engineering Department, Tufts University, Medford, Massachusetts 02155, United States

Supporting Information

ABSTRACT: Membranes that can separate molecules of similar size based on chemical features could transform chemical manufacturing. We demonstrate membranes with functional, 1−3 nm pores prepared using a simple and scalable approach: coating a porous support with random copolymer micelles in alcohol, followed by precipitation in water and functionalization of pore surfaces. This approach was used to prepare membranes that can separate two hormones of similar size and charge, differentiated by aromaticity, mediated through $\pi-\pi$ interactions between the aromatic solute and pore walls functionalized with phenol groups. The aromatic molecule permeates more slowly in single-solute experiments. In competitive diffusion experiments, however, it permeates 7.1 times faster than its nonaromatic analogue. This approach can be used to manufacture membranes for complex separations based on various intermolecular interactions.

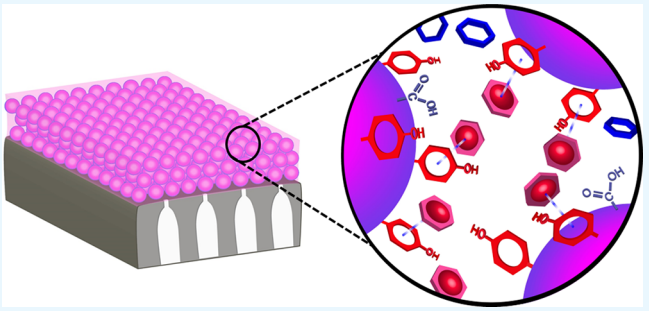

KEYWORDS: *chemoselective membranes, filtration, aromaticity, nanoconfinement, molecular interactions*

INTRODUCTION

Chemical separations account for approximately 10% of the world's energy consumption.[1] Separation of small molecules is particularly energy-intensive, often conducted by distillation, extraction, or chromatography.[2] Membrane filtration is energy-efficient and simple and requires no added chemicals,[3−5] but its use is mostly limited to size-based separations.[6,7] Developing highly selective membranes that can separate molecules of similar size on the basis of their structure would transform chemical and pharmaceutical manufacturing, significantly cutting the energy use and carbon emissions associated with separations.[1,8] Such materials would also impact drug delivery, sensors, and barrier materials.[9,10]

Most commercial membranes on the market today broadly rely on size-based sieving of particles and solutes.[6] Nanofiltration (NF) and reverse osmosis (RO) membranes, designed for removing salts from water, typically possess negatively charge surface to enhance rejection and reduce fouling.[8] Hence, they show some degree of charge-based separation through the Donnan exclusion mechanism.[11] Hydrogen bonding, polarity, and hydrophobicity can also play a role in the organic solute selectivity of commercial NF and RO membranes.[12−15] Nonetheless, size exclusion is still the most dominant and well-understood separation mechanism in these and other commercial membranes.[15−17] Importantly, the effects of these other factors are typically not well controlled or consistent enough to enable their use for the reliable, purposeful separation of organic molecules of similar size.

In contrast, biological pores such as porins and ion channels exhibit exceptional selectivity combined with fast and efficient permeation. These features arise from confining flow into constricted pores, comparable in size with the target solute (∼1 nm for small molecules), lined with functional groups.[18] Solutes that favorably and reversibly interact with the pore walls are preferentially partitioned into the nanopores and permeate through while preventing the entry of other solutes.[19] For instance, maltoporin, an outer membrane protein found in bacteria, can selectively transport maltooligosaccharides over other oligosaccharides.[20] Its structure exhibits residues that selectively bind maltotriose,[21] and permeation studies show that binding affinity has a significant effect on transport properties.[20,22] Similar behavior is observed in other bacterial outer membrane proteins[23] as well as the nuclear pore complex.[24] Although the sizes of solute (and thus pores) vary greatly, the commonalities in how these highly selective pores function remain. This implies that synthetic membranes with <3 nm pores lined with properly selected functional groups can potentially separate organic molecules of similar size but different chemical features.

Most approaches to prepare such membranes involve narrowing and functionalizing pores of commercial membranes.[25−29] These studies demonstrate that separations based on size, charge, hydrophobicity, and chirality can be achieved. However, their broader use is limited because of complex

Received: January 2, 2019
Accepted: March 7, 2019
Published: March 7, 2019

DOI: 10.1021/acsami.9b00090
ACS Appl. Mater. Interfaces 2019, 11, 12854−12862

Scheme 1. Schematics of (a) Chemical Structure of the Copolymer; (b) Membrane Structure, with a Selective Layer Formed of Tightly Packed Micelles; (c) Unfunctionalized Membrane Nanopores Lined with COOH Groups; and (d) Proposed Membrane Selectivity Mechanism in a Competitive Permeation Experiment with Membrane Functionalized with Phenol Groups

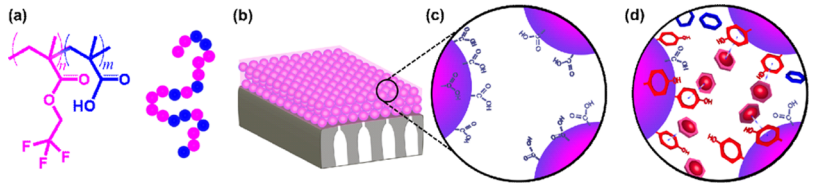

fabrication processes and the very low porosity of resultant membranes.

Generating functional nanopores by self-assembly can offer simpler, more scalable manufacture and higher pore density and permeability. Block copolymers can form membranes with ordered, functionalizable structures,[30] including through elegant, highly scalable processes.[31−33] Nonetheless, it is extremely difficult to create <5 nm pores for small-molecule separations.[34] Block copolymer self-assembly itself typically results in relatively large pores, so additional processing steps are required to reduce their size. For instance, if membranes are prepared from block copolymers to form pores lined with a polyelectrolyte, these pores can be shrunk down to ∼1 nm by causing these chains to expand into the pores in response to pH.[35] The pH and ionic strength stability of this pore size can be further improved by designing a block copolymer that contains strong polyelectrolyte brushes that remain charged and thus extended through the pores.[36] However, the need for particular block chemistry to achieve this smaller pore size with block copolymers also limits the range of functional groups that can be incorporated to control selectivity.

Smaller nanopores can be formed by the self-assembly of small-molecule amphiphiles,[37,38] macrocyclic peptides,[39,40] nanoparticle/dendrimer mixtures,[41] and carbon nanotubes.[42] However, these approaches either involve complex manufacturing methods with poor scalability and/or allow limited chemical functionalizability that restricts the types of possible separations. Only size- and charge-based selectivities have been demonstrated in membranes formed by self-assembly.

Membranes that can separate compounds based on the presence and electron density of aromatic rings are of interest for several applications, from petrochemical processing to the separation of bioactive molecules.[43,44] $\pi-\pi$ interactions between aromatic groups, ubiquitous in biological processes,[45] self-assembly, catalysis, and transport,[46] can be leveraged to differentiate compounds based on aromatic rings. This premise has not yet been explored for membrane-based separations.

Here, we describe the first membranes that can separate organic molecules of similar size and charge based on the presence of an aromatic group, manufactured using simple methods translatable to roll-to-roll manufacturing. First, we prepare membranes whose selective layers consist of a packed array of micelles with carboxylic acid functional surfaces, spontaneously formed by coating a porous support with random copolymer micelles in alcohol.[47] The interstices between the micelles serve as permeation pathways ∼1−3 nm in diameter, lined with carboxylate groups (Scheme 1). Then, we utilized a straightforward, well-established, and efficient conjugation chemistry that utilizes 1-ethyl-3-(3-dimethylaminopropyl) carbodiimide (EDC) and N-hydroxysuccinimide (NHS) (i.e., EDC/NHS chemistry) to functionalize pore walls for controlled solute−wall interactions.[48−50] This enables us to customize the selectivity of the membrane for desired separations while maintaining high surface pore density and permeability. Using this approach, we demonstrate the manufacture of membranes that can separate two steroid hormones of similar size and charge, differentiated by aromaticity, mediated through strong but reversible $\pi-\pi$ interactions between the aromatic solute and pore walls functionalized with tyrosinol. We study the effect of pore wall chemistry on permeation selectivity and link this with quantitative information on wall−solute interactions measured by quartz crystal microbalance with dissipation (QCM-D). Interestingly, although the solutes that interact more strongly with the pore walls permeate more slowly in single-solute experiments, they are preferentially transported through the membrane in competitive diffusion experiments. This phenomenon likely arises from competition between solute molecules to enter into the very small pores, enabling unprecedented aromaticity-based permeation selectivity. Overall, this work introduces a novel platform for custom-designing membranes for targeted separations, utilizing a versatile pore functionalization technique with QCM-D to screen and select desired surface chemistries.

RESULTS AND DISCUSSION

Copolymer Synthesis and Unfunctionalized Membrane Formation. This study utilizes a scalable approach for manufacturing membranes whose selective layers feature a network of carboxylic acid-functionalized nanochannels, formed through the self-assembly of a random copolymer as it is coated onto a porous support.[47] This copolymer, poly(trifluoroethyl methacrylate-*random*-methacrylic acid), P(TFEMA-*r*-MAA), is synthesized by free-radical copolymerization. Incompatibility between the hydrophilic MAA units and the hydrophobic, fluorinated TFEMA segments leads to the formation of micelles in methanol.[51] When a solution of these micelles is coated onto a porous support and immersed into water, they create a selective layer of closely packed micelles.[47] The interstices between the micelles act as pores estimated to be 1−3 nm in diameter based on geometric packing arguments from dry state images of these membranes,[47] lined with carboxylic acid groups available to interact with solutes or for conversion into other moieties upon further functionalization.

To prepare these membranes, we synthesized P(TFEMA-*r*-MAA) following previously reported procedures.[47,51] The copolymer contained 45 wt % MAA (Figure S1, Supporting Information) and had a number-average molar mass of 606 kg mol^{-1} with a dispersity of 1.75 based on polystyrene standards (see the Supporting Information). A 5 wt % solution of the copolymer in methanol was spread onto a commercial UF membrane (PAN400, polyacrylonitrile, nominal MWCO of

DOI: 10.1021/acsami.9b00090
ACS Appl. Mater. Interfaces 2019, 11, 12854−12862

200 kDa, Nanostone) by a doctor blade. After 20 s for solvent evaporation, the membrane was immersed in deionized (DI) water. This resulted in a selective layer formed of self-assembled random copolymer micelles kinetically trapped in a packed array (Figure S2, Supporting Information). This membrane, previously used for charge-based separations,[47] is described as the "unfunctionalized" membrane.

Selection of Surface Functionality and Membrane Functionalization. As an initial demonstration of this approach for designing chemoselective membranes, we focused on leveraging $\pi-\pi$ interactions between preferred solutes and pore walls. $\pi-\pi$ interactions are highly reversible with fast time constants.[52] Their strength can be predictably tuned by selecting substituents on aromatic rings,[53−55] with favorable interactions between electron-rich and electron-poor aromatic rings.[53,55]

Separation of hormones with similar chemical structures is essential for drug manufacture and in analytical applications for clinical diagnosis.[56,57] Thus, we selected two steroid hormones as an example of a pair of solutes with similar size and charge but different aromaticity. Estrone sulfate (ESTR), the most abundant estrogen precursor in blood, has an aromatic ring. Pregnenolone sulfate (PREG), a relative of progesterone, does not have any aromatic rings (Figure 1a). Besides this, ESTR

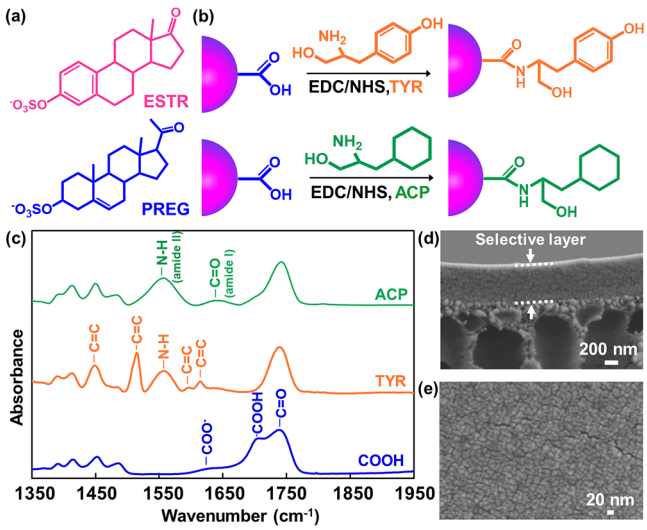

Figure 1. (a) Chemical structures of PREG and ESTR; (b) reaction scheme of membrane functionalization with TYR and ACP; and (c) FTIR spectra of unfunctionalized and functionalized membranes. SEM micrographs of (d) membrane cross section and (e) membrane surface, showing the packed micelle structure intact upon functionalization.

and PREG are very similar in size (8.4 and 8.9 Å, respectively, based on the diameter of a sphere with equivalent volume as calculated by Molecular Modeling Pro software[47,58,59]). These values underestimate the solute size, as this method does not account for solute shape or hydration. However, the model can still provide reliable estimate of relative solute size, as reported previously.[47,58,59] These two hormones also have similar chemical structures and negative charges (−1), so differences in their permeation rates would be due to solute-pore wall interactions.

We hypothesized that if there are aromatic groups lining the membrane pores, only ESTR can interact with them through $\pi-\pi$ interactions. The strength and direction (attractive vs repulsive) of $\pi-\pi$ interactions correlate with the electron densities in the aromatic rings, quantified by Hammett substituent constants, σ_p.[60,61] Rings with electron-donating groups (e.g., phenol; σ_p = −0.37 for −OH) have a partial negative charge and tend to interact more strongly with rings containing electron-withdrawing substituents, such as the OSO_3^- group on ESTR (σ_p = 0.42).[60] Therefore, if we functionalize pore walls with phenol groups, we would expect attractive $\pi-\pi$ interactions between them and ESTR molecules.

To test this hypothesis, we functionalized the membrane pores using EDC/NHS chemistry to covalently attach the phenol-containing molecule tyrosinol (TYR) to the pore walls (Figure 1b). As a control, we functionalized another membrane with a nonaromatic molecule of similar structure, 2-amino-3-cyclohexyl-1-propanol (ACP). TYR-functionalized surfaces are expected to preferentially interact with ESTR over PREG. Unfunctionalized or ACP-functionalized surfaces would not exhibit as a prominent difference in interactions.

Membranes were functionalized in aqueous solution under mild conditions by activating the carboxyl groups to form reactive intermediates (Figure S3, Supporting Information) that then react with an amine to form an amide bond. The procedure was tuned to achieve high degrees of functionalization (see the Supporting Information). Attenuated total reflectance−Fourier transform infrared (ATR−FTIR) spectra for unfunctionalized (COOH) and TYR-functionalized membranes prepared using the optimal procedure (Figure 1c) show almost complete conversion of the carboxylic acid groups and the appearance of aromatic and amide groups, confirming TYR attachment. The spectrum of the ACP-functionalized membrane also shows amide group peaks, indicating successful functionalization. Field emission scanning electron microscopy (FESEM) imaging shows that the closely packed micelles forming the membrane selective layer remain intact after functionalization with TYR (Figure 1d,e). This confirms that this simple, straightforward approach allows functionalization without damage to the membrane nanostructure.

Solute/Pore Wall Interactions that Control Permeation. To confirm our predictions regarding the selectivity of pore−solute interactions and to obtain quantitative evidence of adsorption/desorption equilibria, we used QCM-D. A quartz crystal resonator was coated with a thin film of the copolymer (~70 nm, Figure S4, Supporting Information). Previously, we reported that an array of packed spherical micelles forms upon spin coating a flat mica surface with PTFEMA-*r*-MAA solutions with concentrations of 0.3 wt % and above.[51] On the basis of this, we expect the film on the QCM-D crystal to mimic the membrane surface. Although slight variations of the morphology might exist, this would likely not affect relative adsorption affinities of different solutes on these surfaces. The surface was functionalized with TYR or ACP following the same procedure used for membranes. Frequency change, which is directly proportional to the mass of solute adsorbed on the surface,[62] was recorded upon exposing the crystal to a solution of either PREG or ESTR. For all surfaces, the frequency returned to its initial value upon DI water exposure, indicating immediate and complete desorption of bound solutes (Figure S5a,b, Supporting Information). This shows that the interactions of solutes with functional groups on all of the membranes are fully reversible.

Figure 2 displays the frequency shifts for unfunctionalized (COOH), TYR-functionalized, and ACP-functionalized

DOI: 10.1021/acsami.9b00090
ACS Appl. Mater. Interfaces 2019, 11, 12854−12862

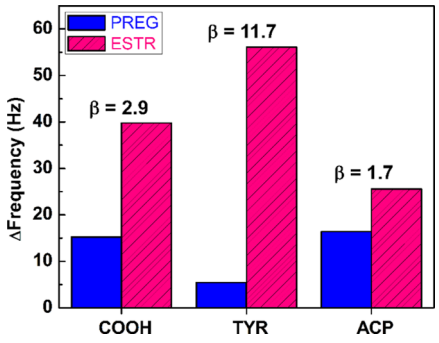

Figure 2. QCM-D frequency shift (n = 3) upon injection of each solute for films featuring different functional groups.

films upon exposure to each solute. All three membranes adsorbed more ESTR than PREG, indicated by a larger frequency shift upon exposure. To evaluate the QCM results more quantitatively, we defined "adsorption selectivity" β as

$$\beta = \frac{\Delta n_{ESTR}}{\Delta n_{PREG}} = \frac{\Delta f_{ESTR}/M_{ESTR}}{\Delta f_{PREG}/M_{PREG}}$$

where Δn denotes moles of each solute adsorbed on the surface, Δf is the frequency shift as a result of interaction with the solute, and M is its molar mass.

The unfunctionalized membrane had an adsorption selectivity β of 2.9. Although no $\pi-\pi$ interactions are present, ESTR can interact more strongly with the −COOH groups on the surface through hydrogen bonding than PREG molecules. This is supported by the hydrogen-bonding solubility parameters of these solutes (Table S1, Supporting Information). The TYR-functionalized surface exhibited a much larger frequency change upon the injection of ESTR, confirming ESTR-TYR affinity through $\pi-\pi$ interactions. In contrast, PREG adsorption was lower in comparison to the unfunctionalized surface. The TYR-functionalized surface was much more selective for ESTR, with a β value of 11.7. The ACP-functionalized surface did not include any aromatic rings, but still had −OH groups available for hydrogen bonding. Frequency shift due to ESTR adsorption was lower than that observed on the unfunctionalized and TYR-functionalized films, whereas PREG adsorption was comparable to the unfunctionalized film. This resulted in a β of 1.7, the lowest preference for ESTR.

Membrane Permeance in Filtration. Most membranes are utilized in pressure-driven filtration applications. Water permeance, water flux normalized by trans-membrane pressure, is a key performance criterion. This value is rarely reported for membranes designed for chemical structure-based selectivity. Membranes prepared by top-down methods often have very low porosity and hence very low permeance. The membranes reported here have much higher pore density, leading to measurable water permeance. The water permeance-unfunctionalized membranes was 4.5 ± 0.8 L m^{-2} h^{-1} bar^{-1}, measured at a trans-membrane pressure of 40 psi, comparable with many commercial membranes.[63]

Upon TYR functionalization, a slight decrease in the membrane permeance to 3.1 ± 0.6 L m^{-2} h^{-1} bar^{-1} was observed as the attached TYR groups partially fill the nanopores. These permeances can be further improved by optimizing the coating process to decrease layer thickness, leading to membranes that operate at industrially relevant fluxes.

Permeation of Aromatic and Nonaromatic Organic Molecules. We first studied the transport of organic molecules through these membranes using diffusion experiments with an aqueous feed containing only one type of solute at a time. We hypothesized that molecular interactions between the solutes and pore walls would control the relative permeation rates of solutes of similar size[19,64] such as ESTR and PREG.

We conducted these diffusion experiments in a two-compartment cell. The feed half-cell was filled with a 0.25 mM solution of desired solute. Samples from the permeate half-cell were assayed using high-pressure liquid chromatography with mass spectroscopy (LC-MS). Figure 3 shows the amount of ESTR (pink circles) or PREG (blue diamonds) permeated through the unfunctionalized (COOH), TYR-functionalized, and ACP-functionalized membranes versus time. We defined theoretical permeation selectivity α_T as the ratio of the permeation rate of ESTR to that of PREG. Both solutes showed very similar permeation rates through the

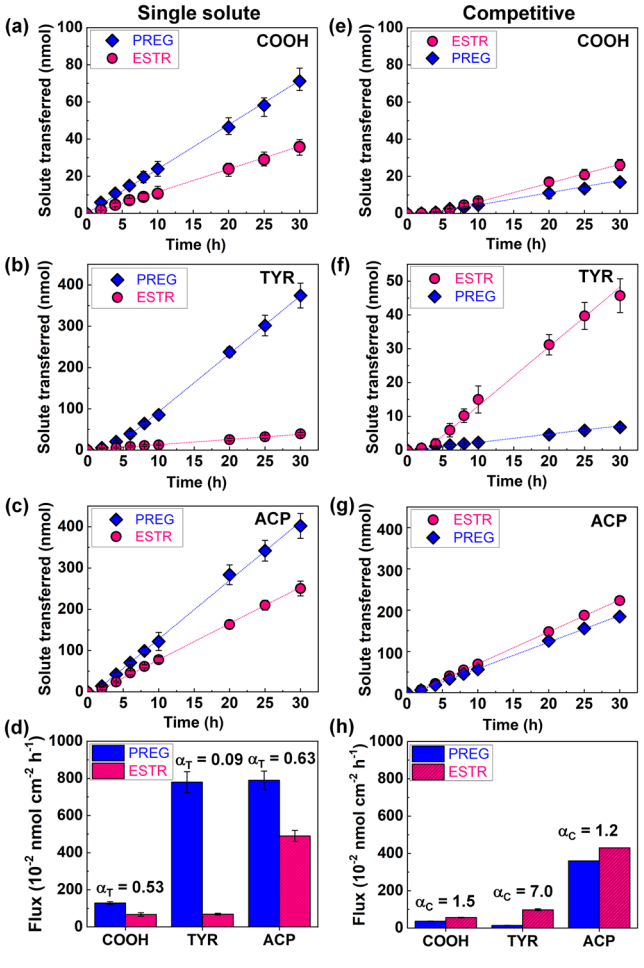

Figure 3. Permeation of steroid hormones in single-solute diffusion experiments through (a) unfunctionalized, (b) TYR-functionalized, and (c) ACP-functionalized membranes. (d) Permeation flux and selectivity in single-solute experiments. Permeation of steroid hormones in competitive diffusion experiments through (e) unfunctionalized, (f) TYR-functionalized, and (g) ACP-functionalized membranes, and (h) flux and selectivity in competitive diffusion experiments.

DOI: 10.1021/acsami.9b00090
ACS Appl. Mater. Interfaces 2019, 11, 12854−12862

support membrane (α_T = 1; Figure S6a, Supporting Information), confirming that these solutes have similar diffusivity.

PREG, the nonaromatic molecule, permeated through the unfunctionalized membrane ~1.9 times faster than aromatic ESTR (α_T = 0.53) (Figure 3a). ESTR interacts slightly more strongly with this membrane than PREG, as indicated by the QCM-D data. These interactions slow down the passage of this molecule as it hops between neighboring binding sites, whereas PREG molecules can pass through the membrane unhindered.[12] Upon functionalization with TYR (Figure 3b), the transport rate of PREG was significantly enhanced relative to the unfunctionalized membrane despite the slightly smaller pore size. This is consistent with the lower degree of adsorption measured by QCM-D and with a decrease in electrostatic repulsion between PREG and the membrane upon the conversion of most of the acid groups to phenol. The transport rate of ESTR increased only slightly in comparison to the unfunctionalized membrane. Although the electrostatic repulsion was reduced, favorable $\pi-\pi$ interactions between TYR and ESTR slow down their permeation. These results are consistent with a hopping mechanism, where adsorption/desorption equilibria dominate the time a solute takes to reach the permeate side.[19] In single solute experiments, the least interactive solute permeates the fastest. Transient trapping of the preferred solute as it hops through the binding sites inside the pores retards its permeation.[12] As a result, PREG diffused 11.2 times faster than ESTR through this membrane (α_T = 0.09).

Both PREG and ESTR diffused faster through the ACP-functionalized membrane compared with the unfunctionalized membrane (Figure 3c) because of the lower membrane surface charge. ESTR diffused slightly more slowly than PREG (α_T = 0.63), in agreement with previous results and QCM-D data. This confirms that the significantly different selectivity observed in the TYR-functionalized membrane arises from $\pi-\pi$ interactions and not from changes in surface charge.

Competitive Permeation with Two Solute Mixtures. Single-solute diffusion experiments are often used to estimate the ability of a new membrane to separate a mixture, presuming that the theoretical selectivity α_T will be maintained when a mixture is fed to the membrane. However, in real applications, the presence of multiple types of solutes might affect permeation selectivity in different ways. In most cases, selectivity either remains similar or decreases (e.g., due to plasticization).[65] In contrast, when the membrane pores are comparable in size to the molecules being separated, the solute with higher affinity to the pore walls can prevent the entry of others into the pore.[19] This results in higher transport selectivity for the preferred solute in comparison with α_T. Therefore, in addition to better simulating realistic operation conditions, comparing data from single-solute and competitive diffusion experiments can illuminate transport mechanisms.

To this end, we performed competitive diffusion experiments with feed solutions containing 0.25 mM for each of ESTR and PREG. We defined competitive selectivity α_C as the ratio of the fluxes of ESTR to PREG, analogous to α_T from single-solute experiments. The support membrane showed essentially no selectivity between the two hormones (α_C = 0.9; Figure S6b, Supporting Information). Interestingly, all three membranes preferentially permeated ESTR, reversing the selectivity observed in single-solute experiments (Figure 3e–g).

The permeation rates of both solutes through the unfunctionalized membrane were lower in the competitive experiment (Figure 3e) than that in single-solute experiments. This decrease was much more pronounced for PREG, making its permeation slightly slower than ESTR (α_C = 1.5). This implies that the ESTR molecules, in which the pore walls preferentially interact with, not only permeate through the membrane at a slightly lower rate compared with single solute experiments (i.e., about 16% decrease in permeation rate, likely due to competition between two solutes of similar size for the channels) but also inhibit the permeation of the unpreferred PREG molecules. The ACP-functionalized membrane also shows a slow-down of PREG permeation and a reversal of selectivity (Figure 3g), but to a lesser extent (α_C = 1.2), in agreement with the QCM-D data.

The most prominent change in selectivity was observed for the TYR-functionalized membrane, which interacts most selectively with ESTR through $\pi-\pi$ interactions. In competitive experiments (Figure 3f), the permeation of PREG was dramatically slower in comparison to single-solute experiments. Interestingly, the permeation of ESTR was enhanced significantly, by about 42% compared with the single-solute experiments, indicating that favorable solute/wall interactions enhance the forward flux of the preferred solute.[47] Overall, ESTR permeated through this membrane 7.0 times faster than PREG. At the end of the experiment, the permeate compartment contained about eight times as much ESTR as PREG, demonstrating the enrichment of the preferred solute. This is a successful separation of a mixture of two very similar molecules, based on a relatively minor chemical structure difference.

The enhanced permeation of the preferred solute (ESTR) and inhibition of the unpreferred solute (PREG) in competitive permeation experiments is in close analogy to biological pores. We hypothesize that this arises from competition between the two solutes to enter the nanochannels, whose diameter (~1–3 nm) is comparable to the size of the solutes (~1 nm). Confinement limits the entry of other molecules once a channel is occupied. ESTR, in which the pore walls preferentially interact with, has a higher probability of partitioning into the pores. They also spend a longer time in the nanochannels, as indicated by their slower permeation in single-solute experiments. This excludes the unpreferred solute, PREG, from entering the pores and slows down its permeation drastically. As a result, ESTR permeates through the membrane faster than PREG when they are both present. Furthermore, it is possible that the PREG molecules that are excluded from the pores accumulate near pore entrance, circumventing the back-diffusion of ESTR molecules and increase their forward flux relative to single-solute experiments.[19]

CONCLUSIONS

This study introduces novel membranes with ~1–3 nm pores whose surface chemistry can be functionalized through an easy conjugation reaction. These membranes are manufactured through simple and scalable methods that can be adapted to roll-to-roll manufacturing, taking advantage of polymer self-assembly. They exhibit industrially relevant water permeances. Using this platform, we demonstrate that in a membrane whose pores are ~1–3 nm in diameter, solute–pore wall interactions can dominate solute transport selectivity. We also demonstrate that QCM-D is an effective method to screen

DOI: 10.1021/acsami.9b00090
ACS Appl. Mater. Interfaces 2019, 11, 12854–12862

these surface/solute pairs in terms of preferential interactions. Our results show that incorporating phenol groups on the walls of the nanopores in this membrane system leads to membranes with excellent aromaticity-based transport selectivity between two steroid hormones with similar size and charge. Interestingly, the confinement of permeation into nanoscale pores leads to a large mismatch in single-solute and competitive transport selectivities. This report is, to our knowledge, the first demonstration of membrane-based separation for small molecules based on their aromaticity. The interesting transport phenomena observed here, not predicted by the commonly used membrane transport models such as the solution-diffusion model, require extensive further experimental and theoretical study. Importantly, how these permeation selectivities correlate with separation in more industrially relevant filtration systems need to be explored.

Beyond this initial demonstration, where $\pi-\pi$ interactions are used to differentiate between steroid hormones, the easy functionalizability of this membrane system enables us to explore the effect of a variety of solute−wall interactions on permeation through nanostructured, functional membranes. It is not hard to imagine designing membranes for each targeted separation by identifying desired functional groups on pore walls, screening them by QCM-D, and easily functionalizing these membranes through EDC/NHS chemistry. As such, this new membrane technology has the promise to become a platform for designing custom membranes for complex separations.

METHODS

See the Supporting Information for expanded experimental methods.

Polymer Synthesis and Characterization. P(TFEMA-*r*-MAA) was synthesized using free-radical polymerization following recently published methods.[47,51] Each of TFEMA and MAA (20 g) and AIBN (0.02 g) were dissolved in 100 mL of dimethyl sulfoxide (DMSO) in a round bottom flask. The flask was sealed and purged with nitrogen for 30 min and then placed in an oil bath set to 55 °C. Polymerization reaction occurred under stirring at 55 °C for about 4 h. The flask was removed from the oil bath and unsealed, and 2 g of MEHQ was added to stop the reaction. Copolymer was recovered by precipitation in a mixture of ethanol and hexane (1:3 v/v), redissolved in ethanol, and washed three times in hexane to remove all monomer residues. The final product was then air dried overnight and dried in a vacuum oven at 50 °C for 24 h. The yield was about 40%.

The synthesized copolymer was characterized using ^{1}H nuclear magnetic resonance (^{1}H NMR) spectroscopy. After dissolving the copolymers in DMSO-d_6, NMR spectra were acquired on a Bruker AVANCE III 500 spectrometer. Molecular weight distribution measurement of the copolymer was acquired using a Shimadzu gel permeation chromatography System equipped with a TOSOH TSK gel GMHh-M mixed-bed column and guard column, equipped with both UV and refractive index detectors. THF was used as the mobile phase at 0.75 mL min^{-1} elution rate and calibrated with low polydispersity poly(styrene) standards (TOSOH, PSt Quick Kit).

Membrane Fabrication and Characterization. The copolymer solutions for membrane preparation were prepared by dissolving 5 wt % of the copolymer in methanol by stirring at 40 °C overnight. Afterward, the solutions were filtered through 1 μm glass fiber syringe filter (Whatman) and kept in an oven at 50 °C for 1 h to eliminate the bubbles.

Bubble/dust-free solutions were cast onto a PAN400 ultrafiltration membrane (polyacrylonitrile, nominal MWCO of 200 kDa) taped on a glass plate with an adjustable doctor blade (Gardco, Pompano Beach, FL) set to a gap size of 20 μm. The glass plate was immersed into a water bath after 20 s of solvent evaporation at room temperature.

The microstructure of the membrane was characterized by Supra 55 FESEM at 3 kV and 7 mm working distance. Dried membranes were frozen in liquid nitrogen and cut with a razor blade for cross-sectional imaging. To avoid charging, the samples were sputter coated (Cressington 108 manual, Ted Pella Inc., CA) with Au/Pd (60/40) for 120 s at 30 mA current in an argon atmosphere.

Attenuated total internal reflectance−Fourier transform infrared (ATR−FTIR) spectroscopy was used to identify the chemical composition of the membranes using a FT/IR-6200 spectrophotometer (JASCO Corp, Tokyo, Japan) over the range of 4000−600 cm^{-1} at a 4 cm^{-1} resolution. Prior to analysis, membranes were air-dried overnight.

Membrane Functionalization. To convert carboxylate groups to desired moieties, carbodiimide chemistry was used. The optimal procedure for conversion of carboxylate groups into reactive intermediates was identified by screening EDC/NHS solutions at various concentrations and immersion times and analyzing the resultant membranes using ATR−FTIR to determine extents of functionalization and side-reactions (Supporting Information). We identified the optimal protocol to be as follows: membranes were first immersed in 50 mM MES buffer at pH 6 for 1 h to deprotonate carboxylic acid groups. Next, the membranes were immersed in a solution containing 100 mM EDC and 200 mM NHS in 50 mM MES buffer containing 0.25 M NaCl at room temperature on a nutating mixer for 2 h. Membranes were then rinsed with 50 mM MES buffer (pH 6) several times. For amine conjugation, the membranes were immersed in 100 mM amine (TYR or ACP) solution in 5× SSC buffer adjusted to pH 8 with 0.1 M NaOH on a nutating mixer for 15 h. Unreacted amines were removed by rinsing the membrane with 2× SSC buffer twice and final rinsing with DI water.

Filtration Experiments. Water permeability was measured using a 10 ml Amicon 8010 dead-end stirred cell (Millipore) with a filtration area of 4.1 cm^2, stirred at 500 rpm, at a trans-membrane pressure of 40 psi. Flux was calculated by monitoring the mass of permeate, collected on a scale (Ohaus Scout Pro) connected to a computer. The membrane permeance (L_p), defined as the flux (J) normalized by applied trans-membrane pressure (ΔP), was calculated as

$$L_p = \frac{J}{\Delta P} = \frac{1}{R_{total}} \quad (1)$$

R_{total} accounts for the resistance toward the flow of the coating and the support membrane itself.

Diffusion Experiments. Permeation studies were performed in a U-shaped two-compartment cell (Permegear) with a cell volume of 7.0 mL and an effective permeation area of 1.8 cm^2. A circular membrane switch 1 in. in diameter was mounted between the two-halves of the diffusion cell: feed and permeate half-cells. Feed half-cell contained a 0.25 mM solution of desired solute (ESTR and PREG), and permeate half-cell was filled with DI water. Aliquots (1 mL) were removed from the permeate solution and replaced with 1 mL of DI water to sustain a roughly constant concentration gradient between the two chambers. The flux of permeating solute through the membranes and into permeate half-cell was monitored by periodically assaying these aliquots using high-pressure liquid chromatography coupled with mass spectroscopy (LC-MS, Finnigan Surveyer LC system and Finnigan LTQ, Thermo Scientific, Waltham, MA). Samples or standards (20 μL) were injected into a C18 Analytical Column (BetaSil C18 Column, 3 μm particle size, 100 mm length, 2.1 mm internal diameter, Thermo Scientific, Waltham, MA) equilibrated with 95:5 water/ACN containing 0.02 v/v % ammonium hydroxide. A gradient was started to 60:40 water/ACN over 5 min. Then, ramped up to 95:5 water/ACN, followed by a 2 min equilibration step.

Quantification was performed by tracking m/z values of 349.2 and 395.2 for ESTR and PREG, respectively. Membranes were soaked in DI water at least overnight between diffusion experiments to remove any organic solute residues.

QCM-D Studies. To study the interaction between the solute and selective layer, we used QCM-D (Q-Sense, Frölunda, Sweden). AT-

DOI: 10.1021/acsami.9b00090
ACS Appl. Mater. Interfaces 2019, 11, 12854−12862

quartz crystals (0.3 mm thick) coated with a 100 nm thick gold layer (QSX 301) with a fundamental frequency of f_0 = 4.95 ± 0.05 MHz were used as substrates. Prior to use, Au-coated crystals were cleaned by UV/ozone treatment for 10 min. They were then heated in a 5:1:1 mixture of ultrapure water, 25 v/v % ammonia, and 30 v/v % H_2O_2 to 75 °C for 5 min. Subsequently, they were rinsed with ultrapure water, blow dried with nitrogen, and placed under UV/ozone treatment for another 10 min.

To obtain a thin and uniform film on the crystal sensor, a solution containing 1 wt % copolymer in methanol was spin-coated at 2000 rpm for 1 min. The samples were then dried in a vacuum oven at 70 °C for 30 min to remove any solvent residue.

For tracking the adsorption and desorption of the solute, frequency change at different harmonics (n = 1, 3, 5, 7, ..., 13) was recorded upon injection of different solutes. The sensor was first equilibrated with ultrapure water until a stable baseline was stabilized. Next, a solution containing 0.1 mM desired solute (PREG or ESTR) was introduced to the measurement cell using a peristaltic pump (Ismatec IPC-N 4) at a flow rate of 50 μL min^{-1} at room temperature. When the adsorption stabilized, as evidenced by a plateau in the signal, the solution was again substituted with ultrapure water to track desorption of the solute and hence the reversibility of the interactions. The next solute was injected afterward, and its adsorption/desorption was compared.

■ ASSOCIATED CONTENT

Supporting Information

The Supporting Information is available free of charge on the ACS Publications website at DOI: 10.1021/acsami.9b00090.

Expanded experimental methods, ^{1}H NMR spectrum of the copolymer, cross-sectional and surface FESEM images of unfunctionalized membrane, FTIR spectra of activated membranes, structure and properties of molecules used to functionalize the membrane and as solutes, measurement of selective layer thickness via QCM-D, and adsorption/desorption of hormones on the selective layer using QCM-D (PDF)

■ AUTHOR INFORMATION

Corresponding Author

*E-mail: Ayse.Asatekin@tufts.edu.

ORCID

Ilin Sadeghi: 0000-0002-3451-0709

Ayse Asatekin: 0000-0002-4704-1542

Notes

The authors declare no competing financial interest.

■ ACKNOWLEDGMENTS

The authors thank Prof. D. Kaplan for access to QCM-D and spin coater, Dr. D. J. Wilbur for technical assistance with LC-MS, and Prof. H. Yi and Dr. E. Liu for helpful discussions on carbodiimide coupling chemistry. We gratefully acknowledge financial support from Tufts University, the Tufts Collaborates program, and the National Science Foundation (NSF) under grant no. CBET-1553661. FESEM imaging was performed at the Center for Nanoscale Systems (CNS), a member of the National Nanotechnology Infrastructure Network (NNIN), supported by the National Science Foundation under NSF award no. ECS-0335765. CNS is part of Harvard University. Analytical and mass spectroscopy facilities at Tufts University are supported by NSF grant no. CHE-0320783.

■ REFERENCES

(1) Sholl, D. S.; Lively, R. P. Seven Chemical Separations to Change the World. *Nature* **2016**, *532*, 435.

(2) Seader, J. D.; Henley, E. J.; Roper, D. K. *Separation Process Principles: Chemical and Biochemical Operations*, 3rd ed.; Wiley: Hoboken, NJ, 2011.

(3) Sadeghi, I.; Aroujalian, A.; Raisi, A.; Dabir, B.; Fathizadeh, M. Surface Modification of Polyethersulfone Ultrafiltration Membranes by Corona Air Plasma for Separation of Oil/Water Emulsions. *J. Membr. Sci.* **2013**, *430*, 24−36.

(4) Sadeghi, I.; Yi, H.; Asatekin, A. A Method for Manufacturing Membranes with Ultrathin Hydrogel Selective Layers for Protein Purification: Interfacially Initiated Free Radical Polymerization (IIFRP). *Chem. Mater.* **2018**, *30*, 1265−1276.

(5) Sadeghi, I.; Govinna, N.; Cebe, P.; Asatekin, A. Superoleophilic, Mechanically Strong Electrospun Membranes for Fast and Efficient Gravity-Driven Oil/Water Separation. *ACS Appl. Polym. Mater.* **2019**, DOI: 10.1021/acsapm.8b00279.

(6) Baker, R. W. *Membrane Technology and Applications*, 2nd ed.; J. Wiley: Chichester ; New York, 2004.

(7) Park, H. B.; Kamcev, J.; Robeson, L. M.; Elimelech, M.; Freeman, B. D. Maximizing the Right Stuff: The Trade-Off Between Membrane Permeability and Selectivity. *Science* **2017**, *356*, No. eaab0530.

(8) Sadeghi, I.; Kaner, P.; Asatekin, A. Controlling and Expanding the Selectivity of Filtration Membranes. *Chem. Mater.* **2018**, *30*, 7328−7354.

(9) Hou, X.; Jiang, L. Learning from Nature: Building Bio-Inspired Smart Nanochannels. *ACS Nano* **2009**, *3*, 3339−3342.

(10) Jackson, E. A.; Hillmyer, M. A. Nanoporous Membranes Derived from Block Copolymers: From Drug Delivery to Water Filtration. *ACS Nano* **2010**, *4*, 3548−3553.

(11) Verliefde, A. R. D.; Cornelissen, E. R.; Heijman, S. G. J.; Verberk, J. Q. J. C.; Amy, G. L.; Van der Bruggen, B.; van Dijk, J. C. The Role of Electrostatic Interactions on the Rejection of Organic Solutes in Aqueous Solutions with Nanofiltration. *J. Membr. Sci.* **2008**, *322*, 52−66.

(12) Shen, M.; Keten, S.; Lueptow, R. M. Rejection Mechanisms for Contaminants in Polyamide Reverse Osmosis Membranes. *J. Membr. Sci.* **2016**, *509*, 36−47.

(13) Nghiem, L. D.; Schäfer, A. I.; Elimelech, M. Pharmaceutical Retention Mechanisms by Nanofiltration Membranes. *Environ. Sci. Technol.* **2005**, *39*, 7698−7705.

(14) Braeken, L.; Ramaekers, R.; Zhang, Y.; Maes, G.; Bruggen, B. V. d.; Vandecasteele, C. Influence of Hydrophobicity on Retention in Nanofiltration of Aqueous Solutions Containing Organic Compounds. *J. Membr. Sci.* **2005**, *252*, 195−203.

(15) Van der Bruggen, B.; Schaep, J.; Wilms, D.; Vandecasteele, C. Influence of Molecular Size, Polarity and Charge on the Retention of Organic Molecules by Nanofiltration. *J. Membr. Sci.* **1999**, *156*, 29−41.

(16) Schaep, J.; Van der Bruggen, B.; Vandecasteele, C.; Wilms, D. Influence of Ion Size and Charge in Nanofiltration. *Sep. Purif. Technol.* **1998**, *14*, 155−162.

(17) Szymczyk, A.; Fievet, P. Investigating Transport Properties of Nanofiltration Membranes by Means of a Steric, Electric and Dielectric Exclusion Model. *J. Membr. Sci.* **2005**, *252*, 77−88.

(18) Mackinnon, R. Pore Loops: An Emerging Theme in Ion Channel Structure. *Neuron* **1995**, *14*, 889−892.

(19) Zilman, A.; Talia, S.; Jovanovic-Talisman, T.; Chait, B. T.; Rout, M. P.; Magnasco, M. O.; Magnasco, M. O. Enhancement of Transport Selectivity through Nano-Channels by Non-Specific Competition. *PLoS Comput. Biol.* **2010**, *6*, No. e1000804.

(20) Kullman, L.; Winterhalter, M.; Bezrukov, S. M. Transport of Maltodextrins through Maltoporin: A Single-Channel Study. *Biophys. J.* **2002**, *82*, 803−812.

(21) Schirmer, T.; Keller, T.; Wang, Y.; Rosenbusch, J. Structural Basis for Sugar Translocation through Maltoporin Channels at 3.1-Angstrom Resolution. *Science* **1995**, *267*, 512−514.

(22) Van Gelder, P.; Dumas, F.; Bartoldus, I.; Saint, N.; Prilipov, A.; Winterhalter, M.; Wang, Y.; Philippsen, A.; Rosenbusch, J. P.; Schirmer, T. Sugar Transport through Maltoporin of Escherichia Coli: Role of the Greasy Slide. *J. Bacteriol.* **2002**, *184*, 2994−2999.
(23) Koebnik, R.; Locher, K. P.; Van Gelder, P. Structure and Function of Bacterial Outer Membrane Proteins: Barrels in a Nutshell. *Mol. Microbiol.* **2000**, *37*, 239−253.
(24) Lim, R. Y. H.; Aebi, U.; Fahrenkrog, B. Towards Reconciling Structure and Function in the Nuclear Pore Complex. *Histochem. Cell Biol.* **2008**, *129*, 105−116.
(25) Nishizawa, M.; Menon, V. P.; Martin, C. R. Metal Nanotubule Membranes with Electrochemically Switchable Ion-Transport Selectivity. *Science* **1995**, *268*, 700−702.
(26) Hulteen, J. C.; Jirage, K. B.; Martin, C. R. Introducing Chemical Transport Selectivity into Gold Nanotubule Membranes. *J. Am. Chem. Soc.* **1998**, *120*, 6603−6604.
(27) Jirage, K. B.; Hulteen, J. C.; Martin, C. R. Nanotubule-Based Molecular-Filtration Membranes. *Science* **1997**, *278*, 655−658.
(28) Velleman, L.; Triani, G.; Evans, P. J.; Shapter, J. G.; Losic, D. Structural and Chemical Modification of Porous Alumina Membranes. *Microporous Mesoporous Mater.* **2009**, *126*, 87−94.
(29) Asatekin, A.; Gleason, K. K. Polymeric Nanopore Membranes for Hydrophobicity-Based Separations by Conformal Initiated Chemical Vapor Deposition. *Nano Lett.* **2011**, *11*, 677−686.
(30) Kaner, P.; Bengani-Lutz, P.; Sadeghi, I.; Asatekin, A. Responsive filtration membranes by polymer self-assembly. *Technology* **2016**, *04*, 217−228.
(31) Phillip, W. A.; O'Neill, B.; Rodwogin, M.; Hillmyer, M. A.; Cussler, E. L. Self-Assembled Block Copolymer Thin Films as Water Filtration Membranes. *ACS Appl. Mater. Interfaces* **2010**, *2*, 847−853.
(32) Nunes, S. P.; Car, A. From Charge-Mosaic to Micelle Self-Assembly: Block Copolymer Membranes in the Last 40 Years. *Ind. Eng. Chem. Res.* **2013**, *52*, 993−1003.
(33) Peinemann, K.-V.; Abetz, V.; Simon, P. F. W. Asymmetric Superstructure Formed in a Block Copolymer via Phase Separation. *Nat. Mater.* **2007**, *6*, 992−996.
(34) Sinturel, C.; Bates, F. S.; Hillmyer, M. A. High χ-Low N Block Polymers: How Far Can We Go? *ACS Macro Lett.* **2015**, *4*, 1044−1050.
(35) Weidman, J. L.; Mulvenna, R. A.; Boudouris, B. W.; Phillip, W. A. Unusually Stable Hysteresis in the pH-Response of Poly(Acrylic Acid) Brushes Confined within Nanoporous Block Polymer Thin Films. *J. Am. Chem. Soc.* **2016**, *138*, 7030−7039.
(36) Zhang, Y.; Mulvenna, R. A.; Qu, S.; Boudouris, B. W.; Phillip, W. A. Block Polymer Membranes Functionalized with Nanoconfined Polyelectrolyte Brushes Achieve Sub-Nanometer Selectivity. *ACS Macro Lett.* **2017**, *6*, 726−732.
(37) Beginn, U.; Zipp, G.; Möller, M. Functional Membranes Containing Ion-Selective Matrix-Fixed Supramolecular Channels. *Adv. Mater.* **2000**, *12*, 510−513.
(38) Gin, D. L.; Lu, X.; Nemade, P. R.; Pecinovsky, C. S.; Xu, Y.; Zhou, M. Recent Advances in the Design of Polymerizable Lyotropic Liquid-Crystal Assemblies for Heterogeneous Catalysis and Selective Separations. *Adv. Funct. Mater.* **2006**, *16*, 865−878.
(39) Chapman, R.; Danial, M.; Koh, M. L.; Jolliffe, K. A.; Perrier, S. Design and Properties of Functional Nanotubes from the Self-Assembly of Cyclic Peptide Templates. *Chem. Soc. Rev.* **2012**, *41*, 6023−6041.
(40) Hourani, R.; Zhang, C.; van der Weegen, R.; Ruiz, L.; Li, C.; Keten, S.; Helms, B. A.; Xu, T. Processable Cyclic Peptide Nanotubes with Tunable Interiors. *J. Am. Chem. Soc.* **2011**, *133*, 15296−15299.
(41) Park, M.-H.; Subramani, C.; Rana, S.; Rotello, V. M. Chemoselective Nanoporous Membranes via Chemically Directed Assembly of Nanoparticles and Dendrimers. *Adv. Mater.* **2012**, *24*, 5862−5866.
(42) Hinds, B. J.; Chopra, N.; Rantell, T.; Andrews, R.; Gavalas, V.; Bachas, L. G. Aligned Multiwalled Carbon Nanotube Membranes. *Science* **2004**, *303*, 62−65.
(43) Capela, E. V.; Quental, M. V.; Domingues, P.; Coutinho, J. A. P.; Freire, M. G. Effective Separation of Aromatic and Aliphatic Amino Acid Mixtures Using Ionic-Liquid-Based Aqueous Biphasic Systems. *Green Chem.* **2017**, *19*, 1850−1854.
(44) Leuchtenberger, W.; Huthmacher, K.; Drauz, K. Biotechnological Production of Amino acids and Derivatives: Current Status and Prospects. *Appl. Microbiol. Biotechnol.* **2005**, *69*, 1−8.
(45) Fasan, R.; Dias, R. L. A.; Moehle, K.; Zerbe, O.; Obrecht, D.; Mittl, P. R. E.; Grütter, M. G.; Robinson, J. A. Structure-Activity Studies in a Family of β-Hairpin Protein Epitope Mimetic Inhibitors of the p53-HDM2 Protein-Protein Interaction. *ChemBioChem* **2006**, *7*, 515−526.
(46) Meyer, E. A.; Castellano, R. K.; Diederich, F. Interactions with Aromatic Rings in Chemical and Biological Recognition. *Angew. Chem., Int. Ed.* **2003**, *42*, 1210−1250.
(47) Sadeghi, I.; Kronenberg, J.; Asatekin, A. Selective Transport through Membranes with Charged Nanochannels Formed by Scalable Self-Assembly of Random Copolymer Micelles. *ACS Nano* **2018**, *12*, 95−108.
(48) Hermanson, G. T. *Bioconjugate Techniques*, 2nd ed.; Academic Press, 2008; pp 1−1202.
(49) Liu, E. Y.; Jung, S.; Yi, H. Improved Protein Conjugation with Uniform, Macroporous Poly(acrylamide-co-acrylic acid) Hydrogel Microspheres via EDC/NHS Chemistry. *Langmuir* **2016**, *32*, 11043−11054.
(50) Liu, E. Y.; Jung, S.; Weitz, D. A.; Yi, H.; Choi, C.-H. High-Throughput Double Emulsion-Based Microfluidic Production of Hydrogel Microspheres with Tunable Chemical Functionalities toward Biomolecular Conjugation. *Lab Chip* **2018**, *18*, 323−334.
(51) Sadeghi, I.; Asatekin, A. Spontaneous Self-Assembly and Micellization of Random Copolymers in Organic Solvents. *Macromol. Chem. Phys.* **2017**, *218*, 1700226.
(52) Lobert, M.; Bandmann, H.; Burkert, U.; Büchele, U. P.; Podsadlowski, V.; Klärner, F.-G. Dynamics in Host-Guest Complexes of Molecular Tweezers and Clips. *Chem.—Eur. J.* **2006**, *12*, 1629−1641.
(53) Wheeler, S. E. Substituents Effect in π-Stacking Interactions. In *Noncovalent Forces, Challenges and Advances in Computational Chemistry and Physics*; Scheiner, S., Ed.; Springer International Publishing: Switzerland, 2015; pp 421−442.
(54) Cockroft, S. L.; Perkins, J.; Zonta, C.; Adams, H.; Spey, S. E.; Low, C. M. R.; Vinter, J. G.; Lawson, K. R.; Urch, C. J.; Hunter, C. A. Substituent Effects on Aromatic Stacking Interactions. *Org. Biomol. Chem.* **2007**, *5*, 1062−1080.
(55) Cockroft, S. L.; Hunter, C. A.; Lawson, K. R.; Perkins, J.; Urch, C. J. Electrostatic Control of Aromatic Stacking Interactions. *J. Am. Chem. Soc.* **2005**, *127*, 8594−8595.
(56) Boggs, A. S. P.; Bowden, J. A.; Galligan, T. M.; Guillette, L. J.; Kucklick, J. R. Development of a Multi-Class Steroid Hormone Screening Method Using Liquid Chromatography/Tandem Mass Spectrometry (LC-MS/MS). *Anal. Bioanal. Chem.* **2016**, *408*, 4179−4190.
(57) Nowakowska, J.; Pikul, P.; Ciura, K.; Piotrowicz, J. A Simple TLC and HPTLC Method for Separation of Selected Steroid Drugs. *Cent. Eur. J. Chem.* **2013**, *11*, 1297−1308.
(58) Bengani-Lutz, P.; Converse, E.; Cebe, P.; Asatekin, A. Self-Assembling Zwitterionic Copolymers as Membrane Selective Layers with Excellent Fouling Resistance: Effect of Zwitterion Chemistry. *ACS Appl. Mater. Interfaces* **2017**, *9*, 20859−20872.
(59) Asatekin, A.; Menniti, A.; Kang, S.; Elimelech, M.; Morgenroth, E.; Mayes, A. M. Antifouling Nanofiltration Membranes for Membrane Bioreactors from Self-Assembling Graft Copolymers. *J. Membr. Sci.* **2006**, *285*, 81−89.
(60) Hansch, C.; Leo, A.; Taft, R. W. A Survey of Hammett Substituent Constants and Resonance and Field Parameters. *Chem. Rev.* **1991**, *91*, 165−195.
(61) Lewis, M.; Bagwill, C.; Hardebeck, L.; Wireduaah, S. The Use of Hammett Constants to Understand the Non-Covalent Binding of Aromatics. *Comput. Struct. Biotechnol. J.* **2012**, *1*, No. e201204004.

DOI: 10.1021/acsami.9b00090
ACS Appl. Mater. Interfaces 2019, 11, 12854−12862

(62) Marx, K. A. Quartz Crystal Microbalance: A Useful Tool for Studying Thin Polymer Films and Complex Biomolecular Systems at the Solution-Surface Interface. *Biomacromolecules* **2003**, *4*, 1099−1120.
(63) https://www.sterlitech.com/flat-sheet-membranes-specifications.html (accessed 3/15/2019).
(64) Vannucci, C.; Taniguchi, I.; Asatekin, A. Nanoconfinement and Chemical Structure Effects on Permeation Selectivity of Self-Assembling Graft Copolymers. *ACS Macro Lett.* **2015**, *4*, 872−878.
(65) Staudt-Bickel, C.; Koros, W. J. Improvement of CO_2/CH_4 Separation Characteristics of Polyimides by Chemical Cosslinking. *J. Membr. Sci.* **1999**, *155*, 145−154.

DOI: 10.1021/acsami.9b00090
ACS Appl. Mater. Interfaces 2019, 11, 12854−12862